Post-eruptive Persistent Cooling Beneath the Summit Crater of Usu Volcano as Revealed by Magnetic Repeat Surveys

Takeshi Hashimoto[*†]

[*]Institute of Seismology and Volcanology, Faculty of Science, Hokkaido University, N10W8, Kita-ku, Sapporo, Japan
[†]Corresponding author, E-mail: hasimoto@sci.hokudai.ac.jp

Remarkable and continuous geomagnetic field change suggesting remagnetization at a shallow depth was detected by repeated campaigns of geomagnetic field observation in the summit area of Mt. Usu Volcano from 2008 to 2021. Long-term cooling of the remnant magma that intruded during the 1977-82 eruption was considered responsible for the remagnetization. A magnetic dipole parallel to the present geomagnetic field well reproduced the observation. The modeled source was located near the Ginnuma crater, southside of the previously inferred intrusive body beneath the Usu-Shinzan cryptodome. Meanwhile, no magnetic source was detected on the other side of the intrusion, implying the asymmetric heat transport paths around the intrusion. Considering the previous studies on seismicity, geodetic modeling, and resistivity structure, the magnetic source region is plausibly a high permeability zone through which heat from the intruded magma has been efficiently transported. In other words, the source region can be a key monitoring target for a future eruption as it may be linked to the subsurface magma system.

Keywords: geomagnetism, total field, remagnetization, cooling, Usu Volcano

1. Introduction

Changes in temperature and stress states in the subsurface caused by volcanic activity can alter the strength and direction of the magnetization of rocks composing the volcanic edifice. For example, when the remanent magnetization of rocks just below the active crater disappears due to heating, the surrounding magnetic field is distorted, which we can detect with a magnetometer on the ground. Many such cases have been reported in the past and are called volcano-magnetic effects (e.g., [1] [2] [3]).

Reference [1] demonstrated that the geomagnetic field changes associated with the volcanic activity of Mt. Aso were reasonably explained by a thermal demagnetization model. It was pointed out in [1] that the observed changes in the total magnetic field reflected temperature changes in the shallow subsurface. It reported gradual heat build-up and subsequent rapid cooling, respectively prior and posterior to some explosion events. It illuminated a thermal aspect of the typical volcanic behavior associated with an eruption, where we often observe precursory inflation followed by post-eruptive deflation. The thermomagnetic model provided a theoretical basis for interpreting the geomagnetic data monitored at volcanoes. In Japan, geomagnetic observations have been one of the monitoring items of the Japan Meteorological Agency, an official organization to watch domestic volcanic activities. The demagnetization events that were interpreted based on a thermomagnetic effect were reviewed in [4]. Reference [5] gave a typical example of thermal demagnetization during the pre-eruptive processes that lasted for over ten years. As for the long-term remagnetization events, the events observed at Mt. Kuju [6], Mt. Adatara [7], and Mt. Kusatsu-Shirane [8] were interpreted as cooling remagnetization during the post-eruptive or inter-eruptive periods.

In the case of Mt. Usu, Reference [9] repeatedly performed magnetic surveys in the 2000 eruption site and reported the magnetic field changes from 2003 to 2006. According to their observations, the shallow part of the eruption site underwent continuous remagnetization toward the present geomagnetic direction during this period. They interpreted it as the thermal viscous remanent magnetization (TVRM) associated with a moderately elevated temperature around the eruption site, where reversely magnetized rocks underlay. Mt. Usu has erupted in the past at various sites on the volcanic edifice. However, geomagnetic monitoring at sites other than the 2000 eruption site has not been reported. The summit crater is a particularly important area for monitoring because it has repeatedly experienced medium to large-scale magmatic eruptions in historical times. In addition, it is necessary to understand and evaluate the current state, some 40 years after the 1977-82 eruption, to prepare for the next eruption.

In 2008, in association with the research group of Hokkaido University, the author began monitoring the geomagnetic total magnetic field in and around the summit crater of Mt. Usu. Since 2020, the monitoring has continued with the support of Next Generation Volcano Research of the Ministry of Education, Culture, Sports, Science and Technology. In this paper, I first describe the outline of Usu Volcano in Section 2 and briefly explain the volcano-magnetic effects (especially thermomagnetic effects) in Section 3. Then, in Section 4, I present the results of geomagnetic monitoring up to 2021, show that the continuous remagnetization has been going on just below the summit crater, and estimate the source by

thermomagnetic modeling. Finally, in Section 5, I discuss the interpretation of these observations in comparison with the results of previous studies and conclude that this phenomenon reflects the cooling process of the intruded remnant magma of the 1977-82 eruption.

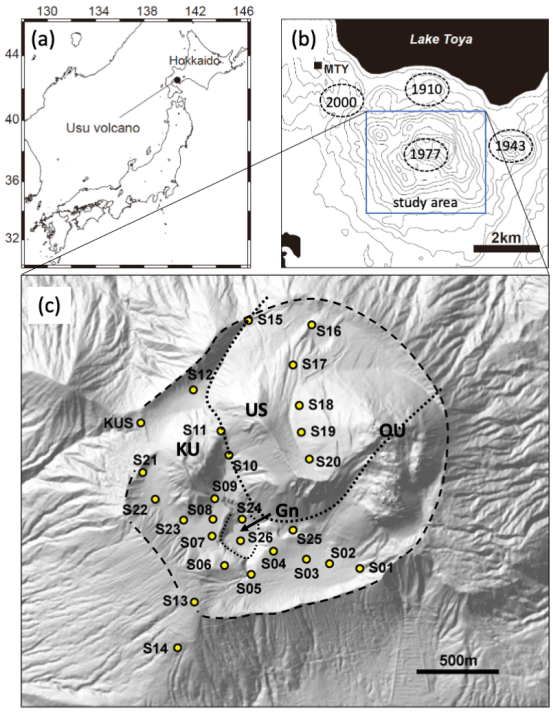

Fig. 1. (a) Location map of Japan showing Usu Volcano. (b) Location map around Usu Volcano. The inset indicates the study area. Dashed circles indicate four eruption sites in the 20th century. (c) A close-up view of the study area showing the magnetic survey sites. The dashed and dotted lines depict the crater rim and the U-shaped fault, respectively. US: The Usu-Shinzan cryptodome, OU: The O-Usu lava dome, KU: The Ko-Usu lava dome, Gn: The Ginnuma crater.

2. Mt. Usu Volcano

Mt. Usu is an active volcano consisting of the central stratovolcano with several lateral cones formed on the southern rim of the Toya Caldera in southwestern Hokkaido 10-20 ka (Figs. 1a, b). The stratovolcano comprises basalt and basaltic andesite with a crater of a 1.8 km diameter atop. After long dormancy following the 7-8 ka summit collapse to the south, Usu resumed its magmatic (rhyolitic to dacitic) activity in 1663. It has erupted nine times since then and four times in the 20th century alone [10]. A variety of eruption sites and eruption styles characterizes the volcano. For example, the most recent eruption was a phreatomagmatic eruption at the western foot of the volcano in 2000, and the eruption in 1943-45 produced a lava dome at the eastern foot. The 1977-82 activity started with four subplinian eruptions at new vents in the summit crater, followed by numerous phreatomagmatic explosions to form the Ginnuma Crater (Gn). It then uplifted the Usu-Shinzan cryptodome (US). O-Usu (OU) and Ko-Usu (KU) are lava domes that emerged from earlier eruptions. In historical times, six of the nine eruptions were magmatic ones from the summit crater, ranging from 2 to 5 in the VEI eruption scale [11].

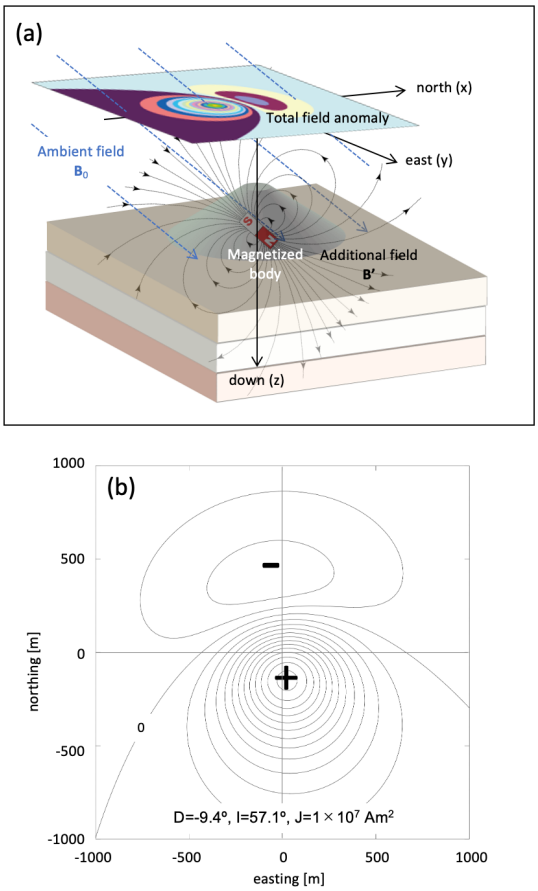

Fig. 2. An example of magnetic anomaly (change). (a) Schematic explanation of a total field anomaly due to a magnetic dipole parallel to the ambient geomagnetic field line. (b) Plan view of the total field anomaly on the observation plane over the volcano shown in the upper panel. The source dipole is placed at (x, y, z) = (0, 0, 500m). Note that the origin is on the observation plane. Contour interval is 1nT. Geomagnetic declination and inclination, and the dipole moment are shown in the panel.

3. Volcano Magnetic Anomaly and Thermomagnetic Effect

Volcanic rocks are generally abundant in ferromagnetic minerals such as magnetite and titanomagnetite, which can be the carriers of the thermal remanent magnetization (TRM) parallel to the geomagnetic field during cooling from magmatic to ambient temperatures. For this reason, volcanic rocks can be considered weak permanent magnets. Thus, the volcanic edifice as a whole behaves like a giant magnet and often accompanies a pair of high and low in the magnetic field intensity called a magnetic anomaly. In addition, the remanent magnetization of rock and the accompanying magnetic field may change with temperature. We term such dependency the thermomagnetic effect. Since volcanic activity is often accompanied by temperature changes in the subsurface, the thermomagnetic effect is one of the essential mechanisms among volcano-magnetic effects. The following is a brief description of the thermomagnetic effect.

In general, the remanent magnetization is often negatively correlated with temperature, even in a temperature range below the Curie point, above which remanent magnetization is perfectly lost. If the rock cools from a high temperature in the presence of the geomagnetic field, it acquires the remanent magnetization (i.e., gets remagnetized) in parallel to the ambient field. Figure 2 explains how magnetic field changes are produced over a volcano. Consider that the volcano undergoes cooling and acquires additional remanent magnetization, represented as a magnetic dipole at a certain depth (Fig. 2a). To consider only the deviation from the initial state, we put a magnetic dipole in parallel to the geomagnetic field within the non-magnetic edifice. Let $\mathbf{B}'(\mathbf{r}, \mathbf{r}')$ be the magnetic field vector at an arbitrary point $\mathbf{r}$ produced by a magnetic dipole at point $\mathbf{r}'$. The actual magnetic field is $\mathbf{B}(\mathbf{r}, \mathbf{r}') = \mathbf{B}' + \mathbf{B}_0$, the vector composite with the ambient field $\mathbf{B}_0$ in this region. As described in the next section, we observe the total magnetic field, which is the intensity of the magnetic field at each measurement site. Therefore, in modeling, we calculate the total magnetic field anomaly $dF(\mathbf{r}, \mathbf{r}') = |\mathbf{B}| - |\mathbf{B}_0|$ at the ground surface. Negative and positive peaks in dF appear on the northern and southern sides of the magnetization source, as shown on the observation plane over the volcano in Fig. 2a. It is because $\mathbf{B}'$ partly cancels $\mathbf{B}_0$ in the north, while it amplifies $\mathbf{B}_0$ in the south. Figure 2b shows a plan view of the magnetic field changes on the plane of observation as an example for the source dipole with a moment of 1×10^7 Am^2 placed at 500 m below the origin. Oppositely, we consider a magnetic dipole antiparallel to the geomagnetic field within the non-magnetic edifice in the case of demagnetization due to heating. In that case, the total magnetic field change has the same pattern as Fig. 2b, with the polarity reversed. The distance between the positive and negative peaks on the

anomaly map roughly reflects how far the source is below the plane of observation. The amplitude of the anomaly is proportional to the magnetic moment of the source.

4. Geomagnetic Monitoring

4.1. Observation

Hokkaido University began geomagnetic field observations in and around the summit crater of Mt. Usu in 2008 (except for KUS, which started in 2007) and has been conducting measurement campaigns since then. The reason for measuring the total magnetic field is that it is more stable and easier to perform than the three-component measurement, and the equipment is relatively accessible. In this study, wooden or plastic pegs, or marks on rocks, are used as measurement points. The measurer moves through the measurement sites in sequence, stands a sensor staff of about 1.2 m long vertically at each site using a spirit level, and takes measurements every 5 seconds for 2 minutes or longer. Usually, the operator can stand the sensor on the same position with an accuracy of a few centimeters by hand without using a tripod. Since we established the measurement points so that the magnetic field gradient was smaller than 100 nTm^{-1}, we considered the maximum measurement error due to misalignment of the sensor position to be a few nT. The instrument used was an Overhauser magnetometer (Gem Systems Inc., GSM-19). The layout of the 27 magnetic points is shown in Fig. 1c. In addition, a reference station was set up at the point about 4 km northwest of the summit crater (MTY: Fig. 1b). During the campaign, continuous measurements were taken at 5-second intervals using the same equipment as the mobile measurement. In the preprocessing stage of the analysis after the data acquisition, I reduced the field fluctuation of extraterrestrial origins by taking the simple difference in the synchronized data between each magnetic point and the reference site. In addition, I visually removed outliers, calculated the average, and used it for the subsequent analysis.

Figure 3 displays the time series of the differential total magnetic field at each magnetic point. At first glance, the variation is generally linear, and the slope has not changed significantly throughout the 13 years from 2008 to 2021. Therefore, I used the linear-fit rate of change in the following analysis. In addition, some measurements are missing due to the loss of the peg. For this reason, the linear fit is done using only the available data and the period used for the fit is not exactly the same among the magnetic points. According to Fig. 3, we see the highest rates around the south side of the Gn crater (S05 and S06).

Cumulative changes at these points exceeded 150 nT over 13 years at the annual rates over 10 nTy^{-1}. The annual rate of the total magnetic field changes observed at each site is mapped in Figs. 4a and 4b. A clear systematic spatial pattern shows positive and negative changes in the southern and northern half of the summit crater, respectively. It is consistent with the characteristics of the dipolar anomaly described in the previous section. The following section attempts source modeling by using magnetic dipole(s).

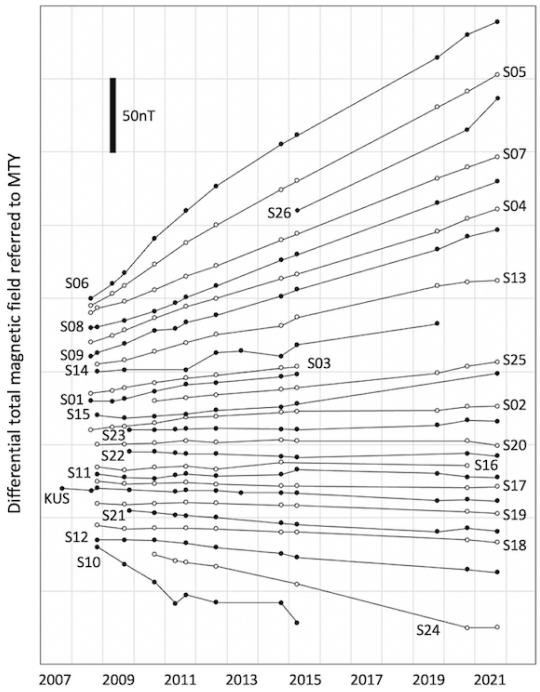

Fig. 3. Differential total magnetic field changes from 2007 to 2021. The reference site is MTY in Fig.1b. Note that difference in marker type of each trace is just for clarity.

Table 1. The optimal model parameters. The equivalent radii are calculated for the spherical sources with magnetization of 0.1 (left) or 1 $Am^{-1}y^{-1}$ (right).

		Model 1 (single source)	Model 2 (double source)
Source 1	X (northing) [m]	-162,287	-162,288
	Y (easting) [m]	47,447	47,495
	Z (elevation) [m]	-144	-79
	J (moment) [Am^2y^{-1}]	1.8×10^{7}	1.4×10^{7}
	equivalent radius [m]	3.5×10^{2}, 1.6×10^{2}	3.2×10^{2}, 1.5×10^{2}
Source 2	X (northing) [m]	N/A	-162,117
	Y (easting) [m]	N/A	47,535
	Z (elevation) [m]	N/A	382
	J (moment) [Am^2y^{-1}]	N/A	-2.4×10^{5}
	equivalent radius [m]	N/A	8.3×10^{1}, 3.9×10^{1}
misfit [nTy^{-1}]		2.62	1.34

4.2. Source Modeling

Here, I describe the procedure of source estimation. First, consider the observed total magnetic field (annual rate of change) d_i at the i-th measurement point (i = 1-N, where N is the total number of sites). Then, let F_i (**r'**, J) denote the modeled total magnetic field anomaly (annual rate of change) due to a subsurface magnetic dipole, at the i-th point. In this study, I used the GRG (generalized reduced gradient) method to minimize the root mean square of the misfit between d_i and F_i, with **r'** (location of the source dipole) and J (annual rate of change in the dipole moment) as the unknown parameters to be searched. The plane rectangular coordinate (PRC) system was used in searching the location. It should be noted that topography does not matter in this modeling because static topographic anomalies are canceled out by taking the differences between campaigns as we only deal with temporal changes at fixed positions.

This study examined the case with a single source (Model 1) and the case with two sources (Model 2). The geomagnetic field declination and inclination used in the models were -9.4º and 57.1º, respectively, referring to the year 2015.0 value at Mt. Usu calculated on the website of the magnetic map of the Geospatial Information Authority of Japan [12]. For Model 2, in which I tried to estimate two sources simultaneously, eight unknown independent parameters made the calculation unstable. Therefore, I adopted the following procedure to deal with this problem. First, I fixed Source 1 of Model 1 and searched Source 2. Next, I fixed Source 2 and made the previous Source 1 free to search again. This procedure was repeated until the parameters of both sources converged. In practice, five iterations of estimation for each source were sufficient to achieve convergence.

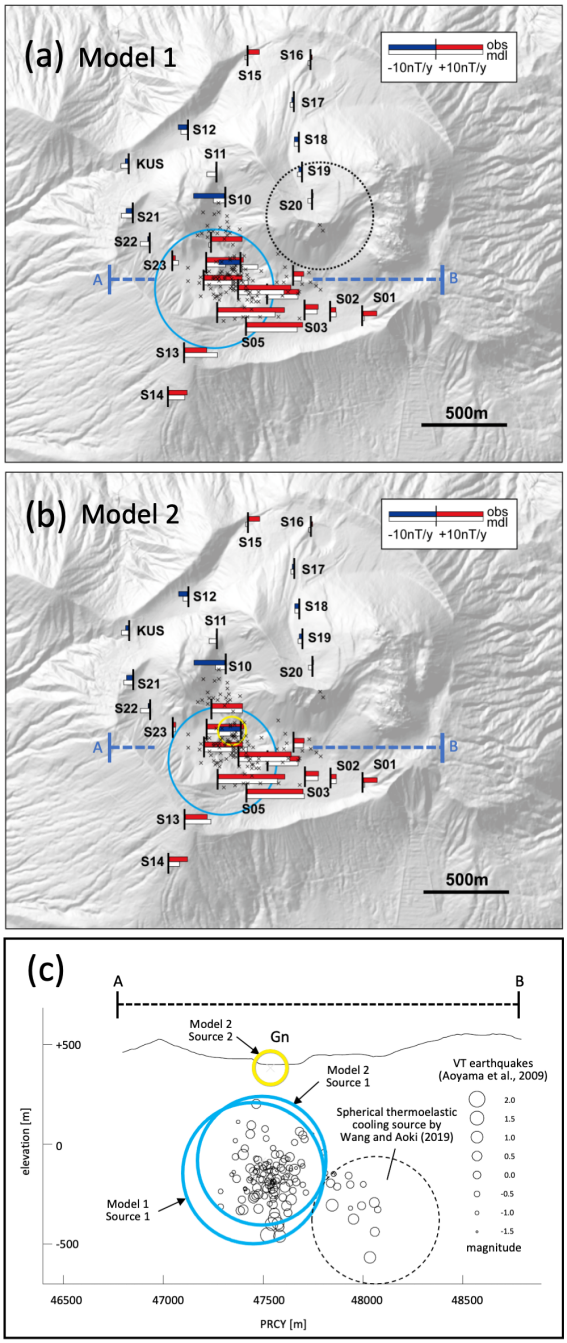

Fig. 4. Summary of Model 1 (panel a) and Model 2 (panel b). Bars at each site show the total magnetic field changes per year. White bars represent the model, while colored ones do observation. Panel c show the EW cross section along the line AB. Circles in cyan and yellow represent the estimated (re/de)-magnetizing sources. Crosses in (a) and (b), and open circles in (c) represent shallow VT hypocenters by [13]. Dashed circles indicate the estimated spherical heat source for the thermoelastic model by [15].

Table 1 summarizes the results of the modeling described above. Figures 4a and 4b display the comparison between the observations and the model estimates at each measurement site. First, let us look at the results of Model 1 (Fig. 4a). The magnetic source is located slightly west of the Gn crater at -144 m altitude. A uniformly magnetized sphere is mathematically equivalent to a magnetic dipole placed at its center. Here, the estimated magnetic moment per year is 1.8×10^{7} Am^2y^{-1}. In the modeling, we cannot independently determine the magnetization (i.e., the magnetic moment per unit volume) and the source volume. Therefore, I present two cases in Table 1 for the source's radius, assuming a uniform magnetization rate of 0.1 and 1 $Am^{-1}y^{-1}$. The cyan and yellow circles in Fig. 4 represent the sources with the former rate assumed since it is more reasonable, as discussed later. At S09, S10, and S24, discrepancies between the observation and the model are relatively large, resulting in the overall RMS misfit of Model 1 being 2.6 nTy^{-1}. It is noteworthy that site S10 is in a valley topography, where occasional

heavy rainfall can cause erosion and deposition of magnetized masses. Therefore, I consider that S10 is less reliable. Meanwhile, the model reproduces 85% of the data at S06, S05, and S26, which are the top three rates of change exceeding 10 nTy^{-1}, indicating that even such a simple model can recover the fundamental features of the anomaly. Measurement points showing systematic negative changes with relatively small amplitudes in the north (except the unreliable S10) also help constrain the model.

Next, let us look at the results of Model 2 (Figs. 4b and 4c). The location and size of the deeper source are almost the same as in the previous case. However, model 2 has an additional weak demagnetization source (Source 2; the yellow circle in Fig. 4b) about 170 m north of Source 1, very close to the ground surface. Although the misfit is yet non-negligible at S10, this model significantly resolves the contradictions at S09 and S24. The overall misfit of the model is 1.3 nTy^{-1}, which is less than 10% of the actual maximum rate of 14.1 nTy^{-1} (S06). However, as mentioned earlier, the calculation becomes unstable when estimating two sources simultaneously. In addition, there are several choices for Source 2, including polarity reversal, that give a similar degree of the misfit.

For this reason, I consider that Model 2, especially regarding Source 2, is not sufficiently constrained by the observed data. In any case, Source 2 is so shallow and weak that it only affects the surrounding area nearby. In other words, Source 2 does not significantly impact the overall model. Meanwhile, for the same reason, non-volcanic terrain changes such as erosion or sedimentation can be the candidate phenomena. Therefore, in this study, I consider it is inappropriate to discuss Source 2 in relation to volcanic activity, and focus the following discussion on Model 1, in which the source parameters are converged firmly.

To evaluate the robustness of the model, I shifted the source position from the best-fitted one in Model 1 (Table 1) and again searched for the least-squares solution by varying the depth and J, the source moment. Figure 5a shows the misfit map around the optimal solution at $\Delta X=\Delta Y=\Delta Z=0$, where X, Y, and Z denote northward, eastward, and downward, respectively. The contours have a slightly shorter axis in the X direction than in Y, meaning that the model is better constrained along the north-south direction. It is reasonable because the positive and negative peaks of a bipolar anomaly align in the geomagnetic north-south direction. Figures 5b and 5c show the profiles at $\Delta Y=0$ and $\Delta X=0$, respectively. Besides the error estimation above, I shifted the optimal source in the Z direction, and searched for the least-squares solution by varying X and J. Figure 5d shows the misfit profile in the Z direction. In Figs. 5b and 5c, the misfit of 3.0 nTy^{-1} roughly corresponds to the inflection points of the curves, below which data fit is not significantly improved further. Therefore, I consider that the error range of the model is about ±100 m and ±150 m in the X and Y direction, respectively. When we adopt the same misfit threshold of 3.0 in the Z direction (Fig. 5d), the error range is from ca. -350 to +200 m, corresponding to an elevation of about -500 to +50 m. The poorer constraint in the Z direction than those in horizontal directions is due to the trade-off between the source depth and strength.

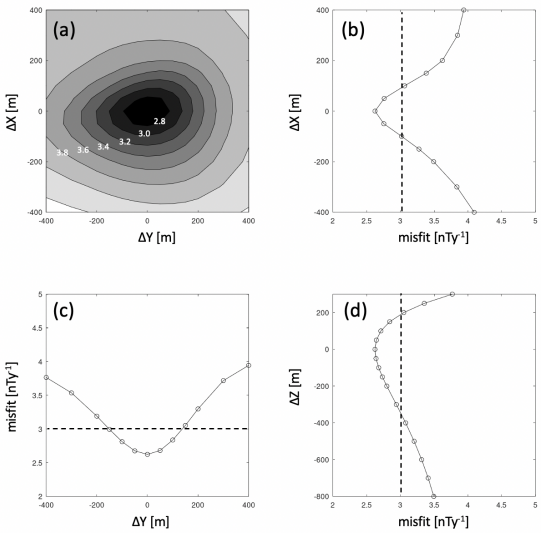

Fig. 5. (a) Distribution of model misfit in which the source is shifted from the best-fit one ($\Delta X=\Delta Y=\Delta Z=0$). (b) Misfit profile along X at $\Delta Y=0$. (c) Misfit profile along Y at $\Delta X=0$. (d) Misfit profile in the vertical direction. Dashed lines indicate the misfit level at 3.0 nTy^{-1}.

5. Discussion

5.1. Thermal Remagnetization Associated with Cooling of the Remnant Magma

Here, I interpret the remagnetizing source in Model 1 estimated in the previous section. The remagnetization center is about 150 m below sea level, almost directly below the Gn crater. It overlaps with the cluster of the volcano-tectonic (VT) earthquakes occurring in this region as a background activity. The hypocenters shown here represent the shallow VT events

recorded by the temporary dense seismic network in 2006[13]. They are determined based on the three-dimensional P-wave velocity structure revealed by an artificial seismic survey[14] and are more accurate and reliable than routine processing. Reference [13] found that these VT events were located along the U-shaped fault surrounding the Usu-Shinzan cryptodome lifted during the 1977-82 eruption. The focal mechanism of the major events suggested that the inner block of the U-shaped fault was subsiding, which agreed well with their InSAR analysis and GNSS data. It should be noted that an intensive dome growth was observed as well as the seismicity with thrust-type focal mechanisms along the U-shaped fault during the previous eruption in 1977-82 ([13] and references within). The earthquakes during the doming are believed to be stick-slip motions because their waveform resembles each other, and the mechanism and timing coincide well with the deformation.

Reference [15], through an intensive InSAR analysis study, found that the Usu-Shinzan continued to subside and that the rate was slowing down with time. They interpreted the subsidence as thermal contraction due to the cooling of the intruded magma during the 1977-82 activity. Their thermoelastic modeling estimated the source as a cooling sphere of (132.18±5.21) $\times 10^6$ m^3 at 396±29 m b.s.l. A dashed circle in Fig. 4c represents their heat source. Note that the sphere center is about 350 m north of this cross-section and that the remagnetization source and the seismic cluster occupy south to southwest of this heat source. Given that their heat source is the intruded magma, then the region of remagnetization should have experienced a rapid elevation in temperature just after the intrusion, followed by a long-term relaxation after the eruption ceased. Because the latter cooling process is still in progress, as suggested by the modeling of [15] and by direct measurements of fumarole temperature [16], it is likely that Source 1 reflects the acquisition of the TRM. Namely, the thermomagnetic effect is a candidate for the mechanism explaining the magnetic field changes we observed. Theoretically, such a relaxation process should obey an exponential-like decay. However, after almost four decades since cooling began, it is no wonder that the latest 13 years look almost linear. Actually, the fumarolic temperature record [16] also shows a quasi-linear trend.

It is noteworthy that our remagnetizing source is off-center from the thermoelastic one. This fact implies that the intruded magma itself is still hot and not in a temperature range for effective acquisition of the TRM, which is consistent with the fact that earthquakes are rare inside the U-shaped fault as rock may not be brittle there. While ground deformation may directly reflect the shrinkage and subsidence of the intrusive body itself, our magnetic field changes seem to indicate a cooling process in the adjacent hydrothermal system. Probably, it is in a temperature range below brittle-ductile transition because we have micro-earthquakes there.

As mentioned earlier, Fig. 4 displays the uniformly remagnetizing spheres with a rate of 0.1 $Am^{-1}y^{-1}$. As a fact of our observation, the magnetization has continued for at least 13 years. Therefore, a simple calculation gives the cumulative magnetization amounting to 1.3 Am^{-1}. If we assume a constant rate for 39 years from the termination of the previous eruption, 1982 to 2021, the cumulative magnetization amounts to 3.9 Am^{-1}. It gives a reasonable value in the same order and smaller than the average magnetization of 5.3 Am^{-1} estimated from an aeromagnetic survey [17] by approximating the edifice uniform. The cumulative magnetization might increase by several factors, considering that the rate decays with time. On the other hand, the rate of 1 $Am^{-1}y^{-1}$ gives a cumulative magnetization of one order higher, suggesting it is unreasonably large. The former case corresponds to the volume of 1.8×10^6 m^3 and the radius of 3.5×10^2 m for Source 1, encircling a large portion of the hypocenters. Note that the above is a crude estimation assuming a spherical source with a uniform rate of remagnetization within it.

5.2. Other Mechanisms

The piezomagnetic effect (e.g., [18]) due to a spherical pressure source can also replicate the pattern in Fig. 2b. However, it must be inflation to match the polarity. It conflicts with the observed ground deformation indicating the continuous deflation in and around the summit crater [15]. Furthermore, assuming the typical stress sensitivity based on laboratory experiments, we need an unrealistically huge pressure change to achieve the observed magnetic field changes over 150 nT. Therefore, I do not consider the piezomagnetic effect plausible in this case.

Next, I consider the possibility of thermal viscous remanent magnetization (TVRM) as another long-term remagnetization mechanism in the thermomagnetic effect. Reference [9] repeated magnetic surveys during 2003-2006, targeting the 2000 eruption site, and found that the shallow subsurface was getting remagnetized at an almost constant rate. They interpreted it as an ongoing acquisition process of the TVRM due to a moderately elevated temperature of the Pleistocene formation with a reversed magnetization. Such a process may be manifested as remarkable magnetic field changes when a reversely magnetized rock gets heated rather than a normally magnetized body. According to the aeromagnetic anomaly map [17], the central stratovolcano of Usu shows no signs of reversed magnetization as a whole. On the other hand, referring to the magnetotelluric resistivity cross-sections in [19], Source 1 lies in the presumed Tertiary formation (Fig. 6), where we cannot rule out the reversed magnetization. However, even in that case, the source region has been subjected to heating by repeated magmatic eruptions in historical times. Then, the reversed magnetization should have already been overwritten. Therefore, I do not consider that the TVRM is a likely cause for the observed magnetic field changes.

5.3. Comparison to Resistivity Model and Hydrothermal Simulation

Reference [19] discussed the time evolution of the magma-hydrothermal system by numerical simulations, assuming the high resistivity (500-1000 Ωm shown as an inverted U in Fig. 6) below Usu-Shinzan in the magnetotelluric 2D cross-section as the remnant magma. The simulation revealed that the intruded magma thermally affected the region within a lateral extent of about 500 m. Our remagnetizing source sits 500 m southwest of the presumed intrusion, coincident with the range of influence. They pointed out that a certain degree of permeability of the host rock was necessary for their simulations to

reproduce the observed heat discharge rate and fumarolic temperature history. Reference [15] also pointed out that the high permeability facilitating an efficient heat transfer by groundwater was necessary to meet a high thermal diffusivity in explaining the long-term ground subsidence by the thermoelastic model.

Source 1 is almost coincident with the area where the shallow VT earthquakes are concentrated and thus is possibly a high permeability fractured zone. In addition, the temperature field seems to be asymmetric around the intrusion because the remagnetization source sits only on the southwest side. The author considers that the uneven and localized distribution of the high permeability paths of heat transport may have contributed to persistent cooling for about 40 years long since the eruption ceased. If this is the case, the Gn crater, including the area nearby, can be a window to the subsurface magma system. One supporting evidence is the previous study by [20] that magmatic diffuse CO_2 soil degassing flux increased around Gn crater about half a year before the eruptive activity in 2000. The activity eventually resulted in the opening of many small craters on the western foot of the stratovolcano. Thus, the magnetic field observation in the summit crater might be one of the helpful tools for detecting a precursory change for the forthcoming eruption of Mt. Usu. However, it should be noted that the magnetic field tends to be less sensitive to the sources of a deep origin. The author also emphasizes that the electrical resistivity model should be updated soon based on a meshed survey, which is one of the ongoing initiatives in the Next Generation Volcano Research. Precise imaging of the presumed intruded magma and its geometry will help better interpret the various monitoring data and evaluate the current state of volcanic activity.

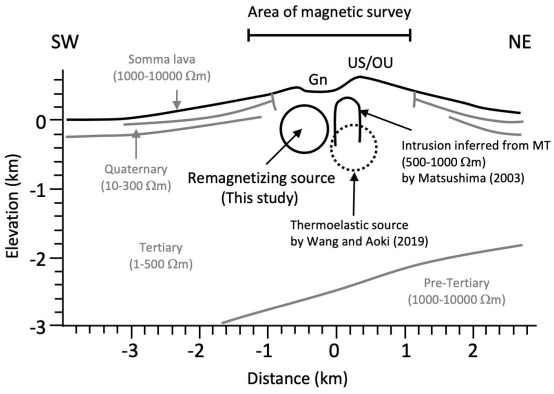

Fig. 6. The remagnetizing source (Source 1 in Model 1) projected on the SW-NE cross section as in Fig.2 of [19]. Resistivity boundaries and the interpretations are also redrawn from [19]. The thermoelastic source by [15] is projected on the same cross section. US: The Usu-Shinzan cryptodome, OU: The O-Usu lava dome, Gn: The Ginnuma crater.

6. Conclusions

In this study, I, in association with other members of Hokkaido University, repeated campaign observations of the total magnetic field in and around the summit crater of Mt. Usu Volcano. I found remarkable and systematic trends at an almost constant rate throughout the observation period from 2008 to 2021. In addition, the records showed a systematic pattern of bipolar changes, suggesting the shallow subsurface was getting remagnetized in parallel to the present geomagnetic field. I searched the source model based on a magnetic dipole by the least-squares method to fit the rate of the field changes at each measuring site. The optimal source was obtained at an elevation about -150 m below the Gn crater. It overlapped the cluster of hypocenters of shallow VT earthquakes[13], where [15] and [19] estimated the latest magmatic intrusion on its northeast neighbor. The author considered that the continuous remagnetizing trend reflected the long-term cooling process in the shallow hydrothermal system adjacent to the intruded magma. Previous studies inferred that the region below the Gn crater was permeable enough to work as the site of effective heat transport. Since I did not detect a similar remagnetization source on the opposite side of the presumed magma, the author considered that the effective heat transport path was localized on the south side of the intrusion.

Acknowledgements

The magnetic campaign observations in this study were performed by the author with the help of many others, including students of Hokkaido University and Sapporo Kaisei High School, other professors, and technical staff of the Institute of Seismology and Volcanology. The author would like to thank them sincerely. The geomagnetic field observation data used in the analysis of this paper are available on the website of the JVDN[21]. This research was partly supported by the Next Generation Volcano Research program of the Ministry of Education, Culture, Sports, Science and Technology of Japan.

References:

[1] Y. Tanaka, “Eruption mechanism as inferred from geomagnetic changes with special attention to the 1989–1990 activity of Aso” Volcano J. Volcanol. Geotherm. Res. Vol.56, pp.319–338, 1993.

[2] R. J. Mueller, M. J. S. Johnston, and J. O. Langbein, “Possible tectonomagnetic effect observed from mid-1989, to mid-1990, in Long Valley Caldera, California” Geophys. Res. Lett., Vol.18, pp.601-604, 1991.

[3] J. Zlotnicki, J. L. Le Mouël, J. C. Delmond, C. Pambrun, and H. Delorme, “Magnetic variations on Piton de la Fournaise volcano. Volcanomagnetic signals associated with the November 6 and 30, eruptions” J. Volcanol. Geotherm. Res. Vol.56, pp.281-96, 1993.

[4] T. Hashimoto, M. Utsugi, T. Ohkura, W. Kanda, A. Terada, S. Miura, and M. Iguchi, “On the source characteristics of demagnetization and ground deformation associated with non-magmatic activity” Bull. Volcanol. Soc. J., Vol.64, No.2, pp.103-119, 2019.

[5] W. Kanda, M. Utsugi, Y. Tanaka, T. Hashimoto, I. Fujii, T. Hasenaka, N. Shigeno, “A heating process of Kuchi-erabu-jima volcano, Japan, as inferred from geomagnetic field variations and electrical structure” J. Volcanol. Geotherm. Res., Vol.189, No.1–2, pp.158-171, 2010.

[6] T. Hashimoto, M. Utsugi, S. Sakanaka, and Y. Tanaka, “Heat Discharging Process and Geomagnetic changes of Iwoyama, Kuju Volcano” Annuals of Disas. Prev. Res. Inst., Kyoto Univ. Vol.45B, pp.617-625, 2002.

[7] T. Yamamoto, A. Takagi, K. Fukui, and T. Owada, “Hydrothermal Activity Inferred from Comprehensive Observation of Unrest in Adatara Volcano” Papers in Meteorol. Geophys., Vol.59, pp.39–64, 2008.

[8] K. Takahashi and I. Fujii, “Long-term thermal activity revealed by magnetic measurements at Kusatsu-Shirane volcano, Japan” J. Volcanol. Geotherm. Res., Vol.285, pp.180-194, 2014.

[9] T. Hashimoto, T. Hurst, A. Suzuki, T. Mogi, Y. Yamaya, and M. Tamura, “The role of thermal viscous remanent magnetisation (TVRM) in magnetic changes associated with volcanic eruptions: Insights from the 2000 eruption of Mt Usu, Japan” J. Volcanol. Geotherm. Res., Vol.176, pp.610-616, 2008.

[10] T. Soya., Y. Katsui, K. Niida, K. Sakai, A. Tomiy, “Geological Map of Usu Volcano 2nd Ed.” Geological Survey of Japan, AIST, 2007.

[11] Japan Meteorological Agency (Ed.), “National Catalogue of the active volcanoes in Japan (4th Ed.), 2013. https://www.data.jma.go.jp/svd/vois/data/tokyo/STOCK/souran_eng/menu.htm [accessed June 16, 2022]

[12] https://vldb.gsi.go.jp/sokuchi/geomag/menu_04/index.html [accessed June 16, 2022]

[13] H. Aoyama, S. Onizawa, T. Kobayashi, T. Tameguri, T. Hashimoto, H. Oshima, and H. Mori, “Inter-eruptive volcanism at Usu volcano: Micro-earthquakes and dome subsidence”, J. Volcanol. Geotherm. Res., Vol.187, pp.203-217, 2009.

[14] S. Onizawa,H. Oshima, H. Aoyam, H. Y. Mori, T. Maekawa, A. Suzuki,T. Tsutsui, N. Matsuwo, J. Oikawa, T. Ohminato, K. Yamamoto, T. Mori, T. Taira, H. Moyamachi, and H. Okada, “P-wave velocity structure of Usu volcano: implication of structural controls on magma movements and eruption locations” J. Volcanol. Geotherm. Res., Vol.160, pp.175–194, 2007.

[15] X. Wang and Y. Aoki, “Posteruptive thermoelastic deflation of intruded magma in Usu volcano, Japan, 1992–2017” J. Geophys. Res. Solid Earth, Vol.124, pp.335–357, 2019.

[16] Japan Meteorological Agency, Usuzan, in National Catalogue of the Active Volcanoes in Japan (The forth edition), 2013. https://www.data.jma.go.jp/vois/data/tokyo/STOCK/souran_eng/volcanoes/015_usuzan.pdf [accessed June 16, 2022]

[17] S. Okuma, T. Nakatsuka, S. Takakura, and R. Morijiri, “Helicopter-borne EM survey over Usu Volcano, Hokkaido Japan, with a special attention to the Usu 2000 eruption” Bull. Volcanol. Soc. Japan, Vol.47, pp.533-546, 2002.

[18] Y. Sasai, “Tectonomagnetic modeling on the basis of the linear piezomagnetic effect” Bull. Earthq. Res. Inst., Univ. Tokyo, Vol.66, pp.585-722, 1991.

[19] N. Matsushima, “Mathematical simulation of magma-hydrothermal activity associated with the 1977 eruption of Usu volcano” Earth Planets Space, Vol.55, No.9, pp.559–568, 2003.

[20] P. A. Hernández, K. Notsu, J. M. Salazar, T. Mori, G. Natale, H. Okada, G. Virgili, Y. Shimoike, M. Sato, N. M. Pérez, “Carbon Dioxide Degassing by Advective Flow from Usu Volcano, Japan” Science, Vol.292, pp.83-6, 2001.

[21] Japan Volcanological Data Network, https://jvdn.bosai.go.jp/app/pages/index.html?root=anyFileEdit&id=d52a79f2-d3df-497f-bc8f-5c512d09b47f [accessed June 16, 2022]